

IMPROVING TIME STABILITY CONSTRAINTS FOR THE SPECTRAL FINITE ELEMENT METHOD IN ACOUSTIC WAVE PROPAGATION NUMERICAL SIMULATIONS

Felipe S. Loureiro^{a,b}, Jonathan E. A. Silva^b and Webe J. Mansur^c

^a*Department of Computer Science, Federal University of Juiz de Fora, 36036-330, Juiz de Fora, MG, Brazil*

^b*Postgraduate Program in Computational Modeling, Federal University of Juiz de Fora, 36036-900, Juiz de Fora, MG, Brazil*

^c*Department of Civil Engineering, COPPE/Federal University of Rio de Janeiro, CP 68506, CEP 21945-970, Rio de Janeiro, RJ, Brazil*

Keywords: acoustic waves, Explicit Green's approach, spectral element, time stepping.

Abstract. The numerical solution of the scalar wave equation, arising, for instance, in geophysics and seismic engineering, by means of the spectral finite element method (SFEM) based on the Gauss-Lobatto-Legendre quadrature has been receiving great popularity. The SFEM can be viewed as a higher-order finite element method (FEM) with some advantages such as mass-lumping and less dispersion errors. However, when common explicit time-stepping schemes are employed, the critical time step becomes too restrictive as the polynomial degree increases. In this context, an explicit time-stepping scheme based on numerical Green's functions is presented to circumvent this drawback. The Green's functions are explicitly computed taking into account the Runge-Kutta (RK) scheme and a time substep procedure. Unlike the standard Runge-Kutta scheme, the present methodology allows the use of large time steps without loss of accuracy. Numerical simulations of a heterogeneous seismic model in an unbounded medium are presented and analyzed in order to illustrate the effectiveness of the proposed formulation.

1 INTRODUCTION

In seismic engineering, the efforts for developing highly accurate numerical techniques for the solution of acoustic and elastic wave equations have been increased.

Finite difference methods, that are the most commonly used approach in this area, may require a large number of grid points to achieve the high accuracy (Virieux, 1986; Kelly and Marfurt, 1990). In practice a balance between numerical accuracy and computational cost is required.

The FEM is often used in engineering but not for seismological studies because of the low accuracy (Komatitsch et al., 2005; Lysmer and Drake, 1972). Although the FEM has advantages for the definition of numerical models such as flexibility in creating meshes owing to the geological structures, the low-order FEM exhibits poor dispersion properties (Marfurt, 1984), while higher-order classical FEM, present some problems such as the occurrence of high oscillations, known as the Runge phenomenon (Boyd, 2001).

Recently, higher-order methods like the SFEM, have been introduced to simulate the acoustic and elastic wave propagation in seismology (Komatitsch et al., 2004). These methods have the geometric flexibility of the FEM, and are able to achieve the expected accuracy using few grid points per wavelength (Komatitsch and Vilotte, 1998). In these methods, the accuracy depends strongly on the choice of the collocation nodal points (Boyd, 2001; Kudela et al., 2007). It is also known, that a limitation of this kind of approach is that the non-uniform points used to construct the algebraic polynomials can place severe restrictions on the time-step length (Khaji et al., 2009).

This paper describes an explicit time-stepping scheme called Explicit Green's Approach that is based on numerical Green's functions (Loureiro and Mansur, 2010; Loureiro, 2011), allowing the use of larger time steps while the accuracy is still maintained. The unbounded domain is simulated by introducing absorbing boundary conditions (Cohen, 2002). At the end of the paper, a numerical example is studied to show the potentialities of the discussed methodology.

2 ACOUSTIC WAVE EQUATION

Time-dependent acoustic problems in a semi-infinite two-dimensional domain are considered here. The unbounded domain is truncated into a computational domain $\Omega \subset \mathbb{R}^2$ surrounded by a smooth boundary $\Gamma = \partial\Omega$. Let $I = (0, T]$ be the time domain of the analysis, the acoustic wave equation considering a nonhomogeneous density can be written as (Morse and Feshbach, 1953; Graff, 1991):

$$\frac{1}{\kappa(\mathbf{x})} \ddot{p}(\mathbf{x}, t) - \nabla \cdot \left(\frac{1}{\rho(\mathbf{x})} \nabla p(\mathbf{x}, t) \right) = b(\mathbf{x}, t), \quad \text{in } \Omega \times I. \quad (1)$$

where ∇ stands for the gradient operator and over dots indicate time derivatives. Furthermore, $p(\mathbf{x}, t)$ denotes the scalar field representing the acoustic pressure, $b(\mathbf{x}, t)$ is the source term, $\rho > 0$ and $\kappa > 0$ are the mass density and bulk modulus, respectively. The velocity c of the wave propagation is given by the relation

$$c(\mathbf{x}) = \sqrt{\frac{\kappa(\mathbf{x})}{\rho(\mathbf{x})}} \quad (2)$$

In addition to Eq. (1), we must supply the initial conditions:

$$p(\mathbf{x}, 0) = p_0(\mathbf{x}), \quad \text{in } \Omega, \quad (3)$$

$$\dot{p}(\mathbf{x}, 0) = q_0(\mathbf{x}), \quad \text{in } \Omega \quad (4)$$

where $p_0(\mathbf{x})$ and $w_0(\mathbf{x})$ are prescribed initial conditions that in geophysics problems both of them are null.

To complete the statement of the problem, the boundary conditions are given by:

$$\alpha(\mathbf{x}, t)p(\mathbf{x}, t) + \beta(\mathbf{x}, t)\frac{\partial p}{\partial \mathbf{n}}(\mathbf{x}, t) + \gamma(\mathbf{x}, t)\dot{p}(\mathbf{x}, t) = g(\mathbf{x}, t), \text{ on } \Gamma \times I \quad (5)$$

where $\alpha(\mathbf{x}, t)$, $\beta(\mathbf{x}, t)$ and $\gamma(\mathbf{x}, t)$ stand for functions to be set according to the choice of the boundary condition, \mathbf{n} is the outward unit normal vector to the boundary and $g(\mathbf{x}, t)$ is the prescribed function on the boundary (e.g., $\alpha = 1, \beta = \gamma = 0$ for a Dirichlet boundary condition). In order to simulate an infinite domain the standard first-order absorbing boundary condition (i.e., $\alpha = 0, \beta = 1, \gamma = 1/c$ and $g = 0$) is employed here (Cohen, 2002). The idea for the absorbing boundary condition is the application of an artificial boundary, that makes the pressure of the reflected wave be zero (Kelly and Marfurt, 1990).

3 EXPLICIT GREEN'S APPROACH (EXGA) EXPRESSION

The major idea of the ExGA method is to adopt the Green's function of the problem under consideration as the test function to enforce the governing equation in a weighted integral sense over the space-time domain $\Omega \times I$. For the acoustic wave propagation problem governed by Eq. (1), the ExGA formulation starts from the following integral statement (Loureiro and Mansur, 2010; Loureiro, 2011):

$$\int_{t_0}^{t^+} \int_{\Omega} \left(\frac{1}{\kappa(\mathbf{x})} \ddot{p}(\mathbf{x}, t) - \nabla \cdot \left(\frac{1}{\rho(\mathbf{x})} \nabla p(\mathbf{x}, t) \right) - b(\mathbf{x}, t) \right) G(\mathbf{x}, \mathbf{y}, t - \tau) \Omega d\tau = 0 \quad (6)$$

where $G(\mathbf{x}, \mathbf{y}, t - \tau)$ is the Green's function of the problem.

The Green's function can be interpreted as the response due to an instantaneous source applied at a point \mathbf{y} (source point) and at an instant τ , which is mathematically represented by $s(\mathbf{x}, t) = \delta(\mathbf{x} - \mathbf{y})\delta(t - \tau)$. Herein, Green's functions that obey homogeneous boundary conditions of the model problem (Eq. (5)) are employed. Thus, the governing equation for the Green's function as well as its boundary and initial conditions read:

$$\frac{1}{\kappa(\mathbf{x})} \ddot{G}(\mathbf{x}, \mathbf{y}, t - \tau) - \nabla \cdot \left(\frac{1}{\rho(\mathbf{x})} \nabla G(\mathbf{x}, \mathbf{y}, t - \tau) \right) = \delta(\mathbf{x} - \mathbf{y})\delta(t - \tau), \text{ in } \Omega, t > \tau, \quad (7)$$

$$\alpha(\mathbf{x}, t)G(\mathbf{x}, \mathbf{y}, t - \tau) + \beta(\mathbf{x}, t)\frac{\partial G}{\partial \mathbf{n}}(\mathbf{x}, \mathbf{y}, t - \tau) + \gamma(\mathbf{x}, t)\dot{G}(\mathbf{x}, \mathbf{y}, t - \tau) = 0, \text{ on } \Gamma, t > \tau \quad (8)$$

$$G(\mathbf{x}, \mathbf{y}, t - \tau) = 0 \text{ in } \Omega, t < \tau, \quad (9)$$

$$\dot{G}(\mathbf{x}, \mathbf{y}, t - \tau) = 0 \text{ in } \Omega, t < \tau. \quad (10)$$

In the ExGA method, the problem domain Ω is partitioned into n_{el} non-overlapping element domains Ω_e , i.e., $\bar{\Omega} = \bar{\Omega}^h = \bigcup_{e=1}^{n_{el}} \Omega_e$ and $\Omega_e \cap \Omega_{e'} = \emptyset$ for $e \neq e'$. Then an approximation for Green's functions and pressure, e.g., $p^h(\mathbf{x}, t) = \sum_i N_i(\mathbf{x}) p_i(t)$ is employed. Thus, after adopting some mathematical steps into Eq. (6) as shown by Loureiro and Mansur (2010); Loureiro (2011), the following expression arises:

$$\mathbf{P}(t) = (\mathbf{G}(t)\mathbf{C} + \dot{\mathbf{G}}(t)\mathbf{M})\mathbf{P}(0) + \mathbf{G}(t)\mathbf{M}\dot{\mathbf{P}}(0) + \int_0^t \mathbf{G}(t - \tau)\mathbf{F}(\tau)d\tau \quad (11)$$

where \mathbf{G} and \mathbf{P} stand for the Green's function matrix and pressure vector, respectively whose entries correspond to their nodal values in the time domain. Moreover, \mathbf{M} , \mathbf{C} and \mathbf{F} (considering $g = 0$) are defined, respectively, as (notice that the integral concerning matrix \mathbf{C} are carried out only along the absorbing boundary).

$$M_{i,j} = \int_{\Omega} N_i \frac{1}{\kappa} N_j d\Omega; \quad C_{i,j} = \int_{\Gamma_A} N_i \frac{1}{\rho c} N_j d\Gamma; \quad F_i = \int_{\Omega} N_i b d\Omega \quad (12)$$

The solution of Eq. (11) is carried out in a step-by-step manner. In this way, splitting the total time analysis I into N equal time intervals, i.e., $[0, T] = \bigcup_{k=0}^{N-1} [t_k, t_{k+1}]$ with $0 = t_0 < t_1 < \dots < t_N = t_f$, $\Delta t = t_{k+1} - t_k = t_f/N$ and $t_{k+1} = (k+1)\Delta t$, Eq. (11) and its time derivative can be written as (Mansur et al., 2007):

$$\begin{aligned} \mathbf{P}^{k+1} &= (\mathbf{G}(\Delta t)\mathbf{C} + \dot{\mathbf{G}}(\Delta t)\mathbf{M})\mathbf{P}^k + \mathbf{G}(\Delta t)\mathbf{M}\dot{\mathbf{P}}^k + \int_0^{\Delta t} \mathbf{G}(\Delta t - \tau)\mathbf{F}(t_k + \tau)d\tau \\ \dot{\mathbf{P}}^{k+1} &= (\dot{\mathbf{G}}(\Delta t)\mathbf{C} + \ddot{\mathbf{G}}(\Delta t)\mathbf{M})\mathbf{P}^k + \dot{\mathbf{G}}(\Delta t)\mathbf{M}\dot{\mathbf{P}}^k + \int_0^{\Delta t} \dot{\mathbf{G}}(\Delta t - \tau)\mathbf{F}(t_k + \tau)d\tau \end{aligned} \quad (13)$$

The above convolution integrals concerning \mathbf{G} and $\dot{\mathbf{G}}$ are approximated by the composite Newton-Cotes rule, yielding (Mansur et al., 2007)

$$\int_0^{\Delta t} \mathbf{A}(\Delta t - \tau)\mathbf{F}(t_k + \tau)d\tau \approx \left\{ \sum_{j=1}^n \left(\frac{1}{2}\psi_1(j) + \frac{1}{2}\psi_1(j-1) \right) \right\} \mathbf{F}^k + \quad (14)$$

$$\left\{ \sum_{j=1}^n \left(\frac{1}{2}\psi_2(j) + \frac{1}{2}\psi_2(j-1) \right) \right\} \mathbf{F}^{k+1} \quad (15)$$

where $\psi_1(j) = \frac{\Delta t}{n} \mathbf{A} \left(\Delta t - \frac{j\Delta t}{n} \right) \left(1 - \frac{j}{n} \right)$, and $\psi_2(j) = \frac{\Delta t}{n} \mathbf{A} \left(\Delta t - \frac{j\Delta t}{n} \right) \frac{j}{n}$, with n being the number of substeps that will be addressed later on subsection 4.2. In a great deal of wave propagation applications, it is quite common to apply only the source term to excite the system that, in most cases, are punctual (or concentrated) sources. In this way, the summations of Eq. (15) are readily evaluated keeping in mind that only Green's functions associated with nodal points of the source function need to be computed.

4 GREEN'S FUNCTIONS COMPUTATION

In this section, the spatial and time discretization of the Green's functions are presented as well as considerations and characteristics of the method.

4.1 Variational formulation and Spatial discretization by the SFEM

To derive the variational form of the problem described by Eqs. (7-10), we start by defining the following discrete space of admissible solutions, where the solution G^h is sought

$$S^h = \{ G^h \in H^1(\Omega) : G^h = 0 \text{ on } \Gamma_1 \times I \text{ and } G^h|_{\Omega_e} \circ \mathcal{F}_e \in \mathbb{P}(\Lambda) \} \quad (16)$$

and the function space V^h of the test functions w :

$$V^h = \{w^h \in H^1(\Omega) : w^h = 0 \text{ on } \Gamma_1 \text{ and } w^h|_{\Omega_e} \circ \mathcal{F}_e \in \mathbb{P}(\Lambda)\} \tag{17}$$

where H^1 is the classical Sobolev space that denotes the space of square-integrable functions with square-integrable generalized first derivatives (Adams and Fournier, 2003).

The discrete Green’s function for a given source point is expressed as $G^h(\mathbf{x}, \mathbf{y}, t - \tau)$, Γ_1 denotes the part of the boundary related to the Dirichlet boundary condition, \mathcal{F}_e is the mapping function between the reference element Λ (biunit square) and a local coordinate system $\boldsymbol{\xi}$ of the element Ω_e , such that $\mathbf{x}(\boldsymbol{\xi}) = \mathcal{F}_e(\boldsymbol{\xi})$ and $\mathbb{P}(\Lambda)$ is taken to be the space generated as the tensor product space of all polynomials of degree $\leq p$ (Canuto et al., 2007; Gopalakrishnan et al., 2007).

Thus, the discrete variational form of the problem reads: find $G^h \in S^h$, such that $\forall t > \tau$ and $\forall w^h \in V^h$ (Hughes, 2000)

$$\left(w^h, \frac{1}{\kappa} \ddot{G}^h\right) + \left(w^h, \frac{1}{\rho c} \dot{G}^h\right)_{\Gamma_A} + a(w^h, G^h) = 0 \tag{18}$$

Notice that the term with respect to the absorbing boundary condition appears in the left hand side of above equation, and the source term was substituted by the follow initial conditions as described by Loureiro and Mansur (2010); Duffy (2001):

$$(w^h, G^h(\mathbf{x}, \mathbf{y}, t - \tau)|_{t=\tau}) = 0 \tag{19}$$

$$\left(w^h, \frac{1}{\kappa} \dot{G}^h(\mathbf{x}, \mathbf{y}, t - \tau)|_{t=\tau}\right) = (w^h, \delta(\mathbf{x} - \mathbf{y})) \tag{20}$$

where (\cdot, \cdot) is the classical L^2 inner product, and the H^1 bilinear form $a(\cdot, \cdot)$ is the inner product described as:

$$a(w^h, G^h) = \int_{\Omega} \frac{1}{\rho} (\nabla w^h \cdot \nabla G^h) d\Omega \tag{21}$$

As described in foregoing equations, the original physical domain Ω is discretized into n_{el} non-overlapping element domains Ω_e , and unknown fields are approximated in the space domain taking into account basis functions $N_i(\mathbf{x})$. Here, the spectral element spatial discretization is considered to construct these basis functions. In fact, the SFEM is characterized by the use of high-order polynomials of degree p in each element.

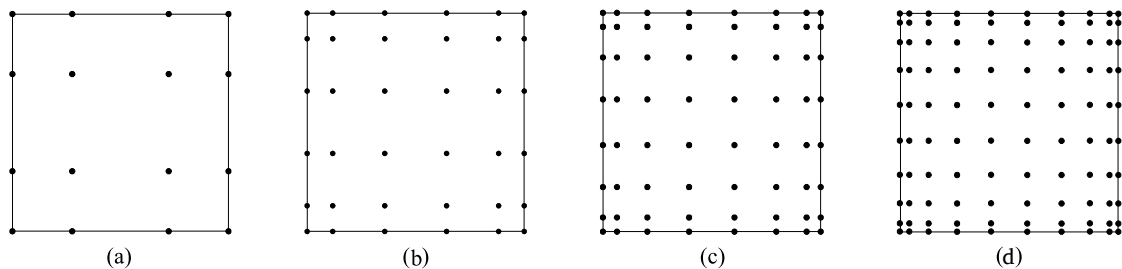


Figure 1: Different kinds of 2D-SFE’s with respect to the polynomial order p : (a) 3×3 ; (b) 5×5 ; (c) 7×7 ; (d) 9×9 .

In this sense, to take advantage of efficient sum-factorization techniques, the set of $(p + 1)^2$ basis points for \mathbb{P} is taken to be the tensor product of the $p + 1$ Gauss-Lobatto-Legendre (GLL) points (the result can be seen in Fig. 1) (Komatitsch and Vilotte, 1998; Komatitsch and Tromp, 1999). Using a numerical quadrature based on the tensor product of 1-D GLL formulas (Zak and Krawczuk, 2011), and choosing the quadrature points to be the same as the basis points, result that for the $p + 1$ quadrature points, all polynomials of degree $\leq 2p - 1$ can be integrated exactly (Komatitsch et al., 1998).

The piecewise polynomial approximation for unknown fields is then defined using the Lagrange interpolation operator on the GLL points, which is the unique polynomial of $\mathbb{P}(\Lambda)$ at the $(p + 1)^2$ basis points. The corresponding basis functions $N_i(\mathbf{x})$ in the reference domain (Λ) are, therefore, the tensor product of two 1D Lagrange interpolants of degree p as clearly seen in Fig. 2 for $p = 7$, constructed as:

$$N_k(\xi, \eta) = l_i^p(\xi)l_j^p(\eta) \quad (22)$$

where $l_i^p(\xi)$ denotes the characteristic 1D Lagrange polynomial of degree p associated with the GLL point i of the corresponding one dimensional quadrature formula.

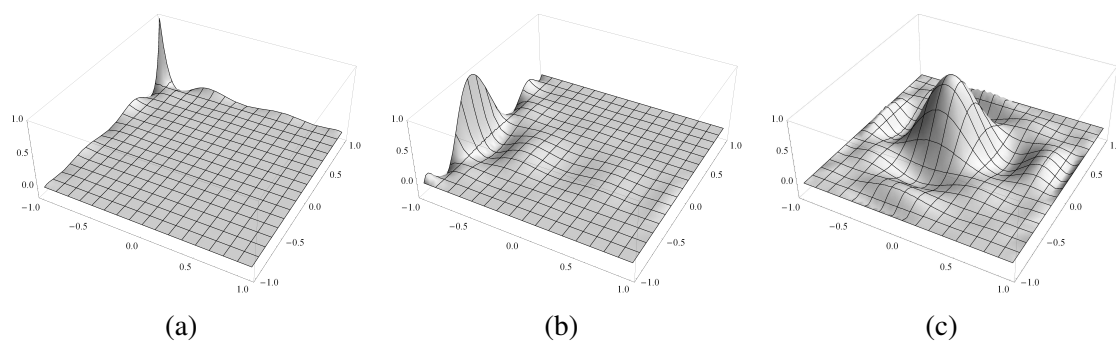


Figure 2: Interpolation functions $N_i(\xi, \eta)$ for the 7×7 SFE: (a) vertex; (b) edge; (c) bubble.

Finally applied this procedure to Eqs. (18-20) leads, like in classical finite element methods (Hughes, 2000), to a system of second-order ordinary differential equations in time (Loureiro, 2011):

$$\begin{aligned} \mathbf{M}\ddot{\mathbf{G}}_j(t) + \mathbf{C}\dot{\mathbf{G}}_j(t) + \mathbf{K}\mathbf{G}_j(t) &= \mathbf{0} \\ \mathbf{G}_j(0) &= \mathbf{0} \\ \dot{\mathbf{G}}_j(0) &= \mathbf{M}^{-1}\mathbf{1}_j \end{aligned} \quad (23)$$

where now $\mathbf{G}_j(t)$ denotes the column j of the Green's matrix with $n_{node} \times n_{node}$ components, n_{node} being the total number of nodes. Matrices \mathbf{M} and \mathbf{C} have already been defined in the previous section and matrix \mathbf{K} is defined as:

$$K_{i,j} = \int_{\Omega} \frac{1}{\rho} \nabla N_i \cdot \nabla N_j d\Omega. \quad (24)$$

Since nodal points are also adopt to perform the numerical integration by the GLL quadrature, it is important to highlight that the mass matrix is naturally diagonal, yielding a very important property from a computational point of view when dealing with explicit time-stepping techniques which is the inversion of the mass matrix in a straightforwardly manner. Notice that this property is not presented in the standard FEM procedure and one needs to rely on special

techniques to lump the mass matrix that for higher order elements leads to some numerical and physical mass conservation problems.

4.2 Time discretization by the RK scheme using substeps

As can be observed in Eq. (13) Green's matrices need to be computed only in the interval $[0, \Delta t]$. These matrices are computed by employing the classical fourth-order RK scheme (Rao and Yap, 1995). Instead of computing them directly from 0 to Δt with just one time step, a substep procedure, where the time step Δt is divided into n equal substeps of length $h = \Delta t/n$, is carried out. This procedure not only improves the precision of the Green's matrices but also increases the stability constraints for the ExGA time-stepping method given by Eq. (13) (Mansur et al., 2007). Hence, when the RK scheme is applied to solve the second order initial value problem expressed by Eq. (23), one obtains the following time recursive expressions (Mansur et al., 2007):

$$\begin{aligned} \mathbf{W}_1 &= \mathbf{M}^{-1} \left(-\mathbf{K}\mathbf{G}^t - \mathbf{C}\dot{\mathbf{G}}^t \right) \\ \mathbf{W}_2 &= \mathbf{M}^{-1} \left(-\mathbf{K} \left(\mathbf{G}^t + \frac{h}{2}\dot{\mathbf{G}}^t \right) - \mathbf{C} \left(\dot{\mathbf{G}}^t + \frac{h}{2}\mathbf{W}_1 \right) \right) \\ \mathbf{W}_3 &= \mathbf{M}^{-1} \left(-\mathbf{K} \left(\mathbf{G}^t + \frac{h}{2}\dot{\mathbf{G}}^t + \frac{h^2}{4}\mathbf{W}_1 \right) - \mathbf{C} \left(\dot{\mathbf{G}}^t + \frac{h}{2}\mathbf{W}_2 \right) \right) \\ \mathbf{W}_4 &= \mathbf{M}^{-1} \left(-\mathbf{K} \left(\mathbf{G}^t + h\dot{\mathbf{G}}^t + \frac{h^2}{2}\mathbf{W}_2 \right) - \mathbf{C} \left(\dot{\mathbf{G}}^t + h\mathbf{W}_3 \right) \right) \\ \mathbf{G}^{t+h} &= \mathbf{G}^t + h\dot{\mathbf{G}}^t + \frac{h^2}{6}(\mathbf{W}_1 + \mathbf{W}_2 + \mathbf{W}_3) \\ \dot{\mathbf{G}}^{t+h} &= \dot{\mathbf{G}}^t + \frac{h}{6}(\mathbf{W}_1 + 2\mathbf{W}_2 + 2\mathbf{W}_3 + \mathbf{W}_4) \end{aligned} \quad (25)$$

Since the RK scheme is an explicit time-marching method, it is only conditionally stable and, as a result, a stability criterion must be satisfied. This property is also transferred to the ExGA method; however, unlike the RK scheme, the ExGA method allows the use of large time steps due to the substep procedure. To better understand this issue, we define the following dimensionless criterion:

$$\frac{c_{\max}\Delta t}{h_{\min}} \leq \beta \quad (26)$$

where c_{\max} is the maximum wave velocity and h_{\min} is the minimum distance between two consecutive nodes. As a generally rule, explicit time-marching methods must satisfy the above criterion for which the parameter β depends on the scheme adopted. For the classical fourth-order RK method we have $\beta = \sqrt{2}$, whereas for the ExGA method the value is $\beta = n\sqrt{2}$ (for comparison purpose notice that $\beta = 1$ for the standard finite central difference method). In this way, the critical time-step length of the ExGA time-stepping method is less restrictive in the sense that one can increase its value by just adjusting the number of time substeps n . In practice, for two or three-dimensional meshes with irregular elements an estimation for the time-step length to assure stability for the ExGA method can be readily calculated as:

$$\Delta t \leq \frac{2n\sqrt{2}}{\sqrt{\lambda_{\max}^e}} \quad (27)$$

where λ_{\max}^e stands for the maximum element eigenvalue in the whole mesh.

The stability constraints of explicit methods is a very important issue when dealing with the SFEM because the nodes are not equidistant and as the polynomial order p increases the distance of the nodes becomes too restrictive as clearly seen in Fig. 1. Indeed, it can be shown that the smallest distance between two nodes in the SFEM behaves as $O(p^{-2})$ (Pozrikidis, 2005), as

a consequence, the higher the value of p , the smaller is the critical time-step length. In such cases, it may be advisable to use implicit time-marching schemes to reduce the number of time steps required for the analysis. Thus, adopting the ExGA method in the analysis, this drawback is circumvented by increasing the number of substeps, and one still has an explicit scheme with all its advantages.

5 NUMERICAL RESULTS AND DISCUSSION

In this section, a numerical example related to wave propagation in geophysics is presented. A computer program and a mesh generator for the SFEM for two-dimensional problems have been developed. The code is able to handle both heterogeneous media and unstructured meshes constructed from the standard FEM quadrilateral element. Furthermore, spectral finite elements with polynomial order up to $p = 9$ (i.e., 9×9 SFE) have been implemented.

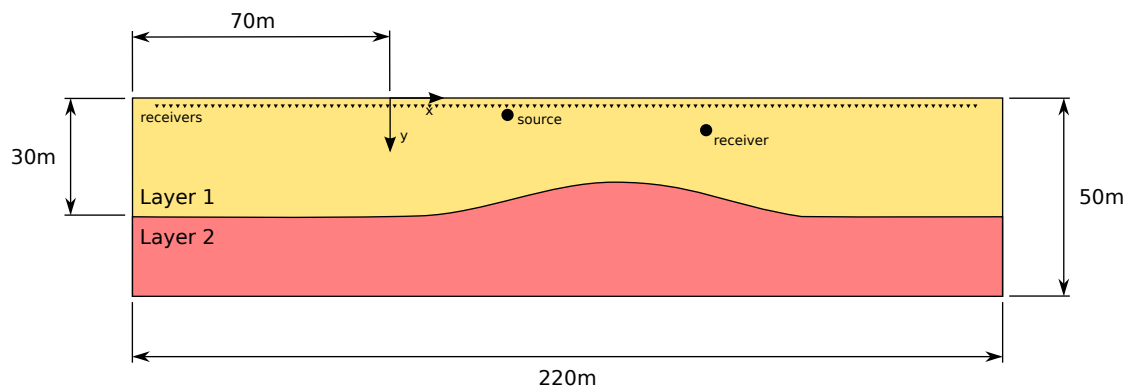


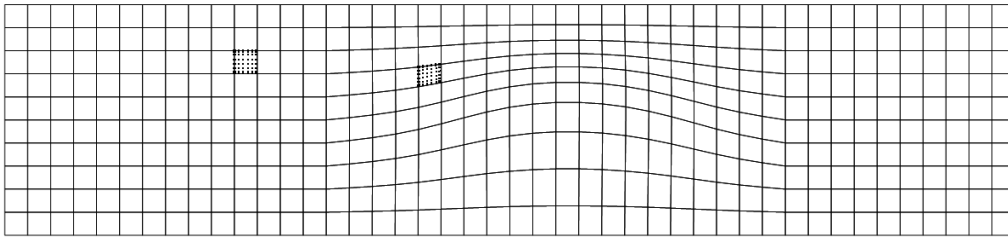
Figure 3: Truncated semi-infinite acoustic model.

The solution of Eq. (1) for a two-layered medium representing a dome raising from the lower layer is analyzed as sketched in Fig. 3. Along the boundary, a null pressure is prescribed at the upper surface, the bottom surface is considered rigid while absorbing boundary conditions are imposed on both sides. The material properties for the two layers are: $\rho_1 = 1000kg/m^3$, $c_1 = 1500m/s$, $\rho_2 = 1500kg/m^3$ and $c_2 = 2100m/s$. The model is excited by a nodal source of Ricker type pulse located at point $(25, -4.65)$ of the form:

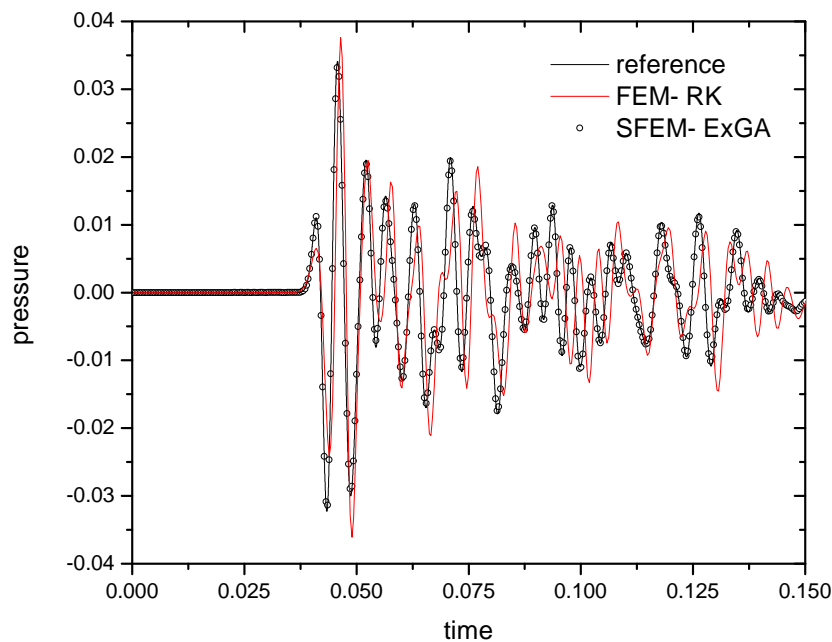
$$\mathcal{R}(t) = -10^{-3} (1 - 2\pi^2 f^2 (t - t_0)^2) e^{-\pi^2 f^2 (t - t_0)^2} \quad (28)$$

where $t_0 = 0.01$ and $f = 160Hz$ stands for the central frequency. As depicted in Fig. 4, the mesh is constructed with $440 \times 7 \times 7$ spectral elements yielding a total of 21939 nodes such that there are at least 5 nodes per smallest wavelength considering the average over all the elements of the mesh, recalling that the cut off frequency is about $400Hz$.

The main goal of this example is to show the ExGA method with substeps can be very efficient in wave problems with the SFEM to increase the time step length for a given analysis. To do so, a comparison between the SFEM and the low-order quadrilateral FEM is examined. The idea is to adopt the same time step length provided by the FEM into the SFEM. A FE mesh composed of 22081 nodes, i.e., approximately the same number of nodes of the SFE mesh, is employed. It is easily verified that the critical time step for the standard RK regarding the FE mesh is $\Delta t \leq 0.00038s$, whereas for the SFE mesh the critical time step is $\Delta t \leq 0.00013s$, i.e., a reduction of about 66% in comparison with that from the FEM. On the other hand, the critical time step for the ExGA method is given by $\Delta t \leq n \cdot 0.00013s$ where the number of substeps

Figure 4: 7×7 SFE mesh

n plays a significant role in its value. Hence, in the present analysis, the chosen time step length is $\Delta t = 0.00036s$ for the FEM and in order to achieve this time step for the SFEM it is required only $n = 3$ substeps into the ExGA method. Since the RK scheme is applied for the time advancement in the FEM, the mass matrix is lumped by taking into account the row sum technique defined as $M_{i,i} = \sum_j M_{i,j}$ (Hughes, 2000).

Figure 5: Pressure time-histories comparison at point $(75, -8.5)$ considering the FEM and SFEM.

Numerical results regarding the FEM with the RK scheme and the SFEM with the ExGA method at the receiver point depicted in Fig. 3 is plotted in Fig. 5. Fig. 5 also shows a reference solution obtained by considering a very fine FEM mesh. It is possible to see that the SFEM-ExGA presents high accuracy results while accompanying the reference solution, differently from the FEM-RK solution which introduces spurious oscillations and large errors into the numerical solution due to the coarse mesh adopted. Thus, the SFEM-ExGA method has the advantage of using the coarse SFE mesh while having a time-step length equal to that of the RK scheme regarding the FE mesh.

To better understand the physical phenomenon concerning the pressure field, Fig. 6 shows the signals recorded along a line of receivers located at $y = -0.25m$ (see Fig. 3). The first record is due to the direct incident wave followed immediately by the reflection at the upper boundary. Then, at time instant of about $0.04s$, the reflected wave originated from the material interface can initially be observed. The reflected wave front originated from the bottom boundary starts to appear at time instant of about $0.068s$. Afterwards, we can see many different wave fronts originated from multiple reflections and diffractions with small amplitudes arriving at the receivers. Fig. 7 shows snapshots of the pressure field taken at three different time instants. The layer boundary is evidenced due to reflections and diffractions at the material interface. On the other hand, Fig. 7c (at left hand side) shows incident waves at the lateral crossing the absorbing boundary.

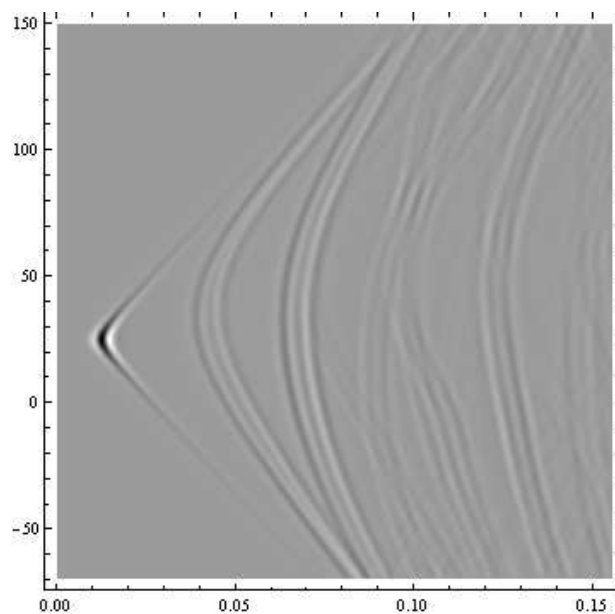


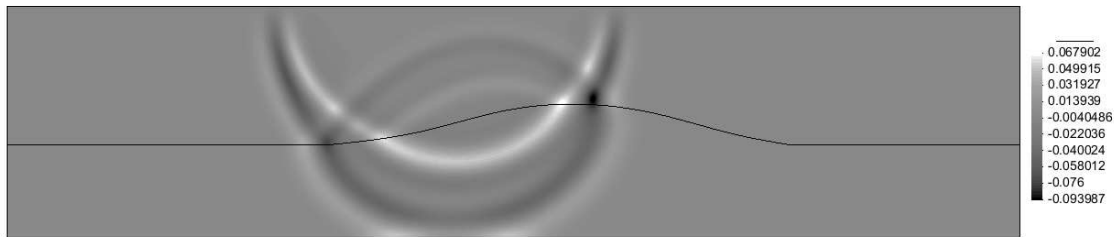
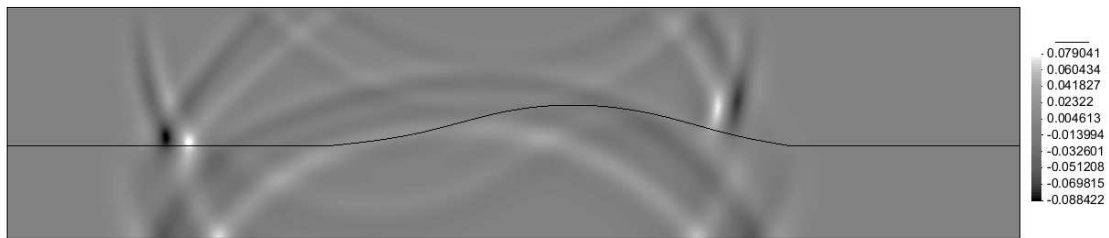
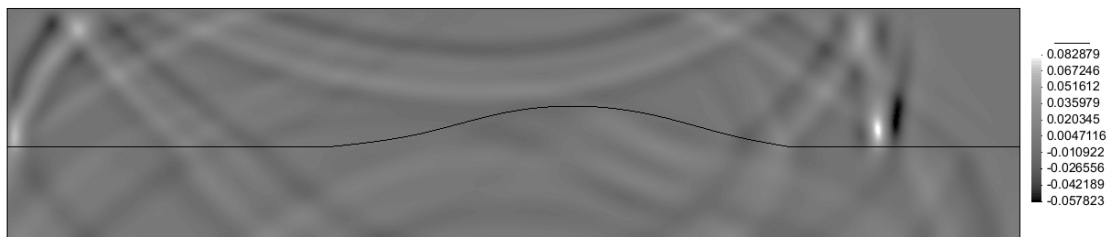
Figure 6: Synthetic seismogram.

6 CONCLUSIONS

In this paper, an explicit time-stepping scheme based on the ExGA method was applied in combination with the SFEM to solve problems governed by the scalar wave equation. The SFEM-ExGA formulation taking into account the fourth order RK scheme shows to be quite effective. This stems from the geometric flexibility offered by the FE mesh together with the spectral element accuracy for using few grid points per wavelength and large time steps furnished by the ExGA method. Thus, having a smaller number of nodes than the standard FEM, the matrices obtained have smaller dimensions, saving on the amount of memory allocated on the computer, enabling us to also work with large-scale problems. The large time step allows us to explore problems with large period of time in a smaller quantity of time steps without loss of accuracy in the results.

7 ACKNOWLEDGEMENT

The financial support of CNPQ, FAPEMIG and UFJF is gratefully acknowledged.

(a) $t = 0.036s$ (b) $t = 0.054s$ (c) $t = 0.07668s$ Figure 7: Snapshots for the pressure field p at different time instants.

REFERENCES

- Adams R. and Fournier J. *Sobolev Spaces*. Pure and Applied Mathematics. Elsevier Science, 2 edition, 2003.
- Boyd J.P. *Chebyshev and Fourier Spectral Methods: Second Revised Edition*. Dover Publications, 2001.
- Canuto C., Hussaini Y., Quarteroni A., and Zang T.A. *Spectral Methods: Fundamentals in Single Domains*. Springer, 2007.
- Cohen G. *Higher-Order Numerical Methods for Transient Wave Equations*. Springer, 2002.
- Duffy D. *Green's Functions with Applications*. Applied Mathematics. Taylor & Francis, 2001.
- Gopalakrishnan S., Chakraborty A., and Mahapatra D.R. *Spectral Finite Element Method: Wave Propagation, Diagnostics and Control in Anisotropic and Inhomogeneous Structures*. Springer, 2007.
- Graff K.F. *Wave Motion in Elastic Solids*. Dover Publications INC., 1991.
- Hughes T.J. *The finite element method: linear static and dynamic finite element analysis*. Courier Dover Publications, 2000.
- Kelly K.R. and Marfurt K.J. *Numerical modeling of seismic wave propagation*. Society of

- Exploration Geophysicists, 1990.
- Khaji N., Habibi M., and Mirhashemian P. Modeling transient elastodynamic problems using spectral element method. *Asian Journal of Civil Engineering*, 10:361 – 380, 2009.
- Komatitsch D., Liu Q., Tromp J., Süß P., Stidham C., and Shaw J.H. Simulations of ground motion in the Los Angeles basin based upon the spectral-element method. *bssa*, 94:187–206, 2004.
- Komatitsch D. and Tromp J. Introduction to the spectral element method for three-dimensional seismic wave propagation. *Geophysical Journal International*, 139:806 – 822, 1999.
- Komatitsch D., Tsuboi S., and Tromp J. The spectral-element method in seismology. In A. Levander and G. Nolet, editors, *Seismic Earth: Array Analysis of Broadband Seismograms*, volume 157 of *Geophysical Monograph*, pages 205–228. American Geophysical Union, Washington DC, USA, 2005.
- Komatitsch D. and Vilotte J.P. The spectral element method: An efficient tool to simulate the seismic response of 2d and 3d geological structures. *Bulletin of the Seismological Society of America*, 88:368 – 392, 1998.
- Komatitsch D., Vilotte J.P., Vai R., Castillo-Covarrubias J.M., and Sanchez-Sesma F.J. The spectral element method for elastic wave equations: application to 2d and 3d seismic problems. *International Journal for Numerical Methods in Engineering*, 1998.
- Kudela P., Krawczuk M., and Ostachowicz W. Wave propagation modelling in 1d structures using spectral finite elements. *Journal of Sound and Vibration*, 300:88 – 100, 2007.
- Loureiro F. *Generalização do método da aproximação explícita de Green para a solução de equações parabólicas e hiperbólicas*. Ph.D. thesis, Universidade Federal do Rio de Janeiro, 2011.
- Loureiro F. and Mansur W. A novel time-marching scheme using numerical Green's functions: A comparative study for the scalar wave equation. *Computer Methods in Applied Mechanics and Engineering*, 199(23):1502–1512, 2010.
- Lysmer J. and Drake L.A. A finite element method for seismology. In *Methods in Computational Physics*, volume 11. Academic Press, New York, 1972.
- Mansur W.J., Loureiro F., Soares Jr D., and Dors C. Explicit time-domain approaches based on numerical Green's functions computed by finite differences—the ExGA family. *Journal of Computational Physics*, 227(1):851–870, 2007.
- Marfurt K. Accuracy of finite-difference and finite-element modeling of the scalar and elastic wave equations. *GEOPHYSICS*, 49:533 – 549, 1984.
- Morse P.M. and Feshbach H. *Methods of theoretical physics*. McGraw-Hill, 1953.
- Pozrikidis C. *Introduction to finite and spectral element methods using MATLAB*. CRC Press, 2005.
- Rao S.S. and Yap F.F. *Mechanical vibrations*, volume 4. Addison-Wesley New York, 1995.
- Virieux J. P-SV wave propagation in heterogeneous media: Velocity-stress finite-difference method. *GEOPHYSICS*, 51:889 – 901, 1986.
- Zak A. and Krawczuk M. Certain numerical issues of wave propagation modelling in rods by the spectral finite element method. *Finite Elements in Analysis and Design*, 47(9):1036 – 1046, 2011.